Mechanism of vibration-induced repulsion force on a particle in a viscous fluid cell

Mehrrad Saadatmand[1,*] and Masahiro Kawaji[1,2,†]

[1]*Mechanical Engineering Department, City College of New York, Convent Avenue at 140th Street, New York, New York 10031, USA*

[2]*Department of Chemical Engineering and Applied Chemistry, University of Toronto, Toronto, Ontario, Canada M5S 3E5*

(Received 17 August 2012; revised manuscript received 8 July 2013; published 19 August 2013)

Space platforms such as the Space Shuttle and International Space Station have been considered an ideal environment for production of protein and semiconductor crystals of superior quality due to the negligible gravity-induced convection. Although it was believed that under microgravity environment diffusive mass transport would dominate the growth of the crystals, some related experiments have not shown satisfactory results possibly due to the movement of the growing crystals in fluid cells caused by small vibrations present in the space platforms called g-jitter. In ground-based experiments, there have been clear observations of attraction and repulsion of a solid particle with respect to a nearby wall of the fluid cell due to small vibrations. The present work is a numerical investigation on the physical mechanisms responsible for the repulsion force, which has been predicted to increase with the cell vibration frequency and amplitude, as well as the fluid viscosity. Moreover, the simulations have revealed that the repulsion force occurs mostly due to the increased pressure in the narrow gap between the particle and the nearest wall.

DOI: 10.1103/PhysRevE.88.023019 PACS number(s): 47.85.−g

I. INTRODUCTION

The near zero gravity environment aboard space platforms such as the Space Shuttle and International Space Station has provided opportunities to investigate certain physical phenomena that could be adversely affected by gravity. For example, the microgravity environment is considered ideal for production of protein and semiconductor crystals of high quality from solutions or melts due to the absence of sedimentation and buoyancy-induced fluid motion. The potential to produce advanced materials has been the motivation behind the crystal growth experiments aboard space laboratories. However, some past experiments have shown unexpected deviations from the ideal diffusion-controlled crystal growth due to the movement of the crystals under microgravity.

Although the protein crystals produced in a fluid cell had been expected to remain suspended and motionless on the space platforms, they have been observed to move in the absence of gravity [1,2]. This could have been due to the presence of accelerations other than gravity which alter the nearly weightless conditions in the space platforms [3]. The major component of vibrations occurs due to the random accelerations and is called g-jitter [4], which is defined as the total contribution to the acceleration field in spacecrafts caused by sources other than gravity. g-jitter can occur due to mechanical vibrations produced by the operation of pumps, fans, and motors, and also by crew motion, spacecraft maneuvers, atmospheric drag, and the Earth's gravity gradient [4–6].

It has been suggested that the unanticipated movements of the particles in protein crystal growth experiments on space platforms is due to the g-jitter vibrations that adversely affect the quality of the crystals during their growth [1,2,7,8]. The g-jitter can induce a hydrodynamic force on a particle suspended in a fluid cell if the densities of the fluid and particle are different. This hydrodynamic force could be observed as an apparent attraction or repulsion force to push the particle towards or away from the nearby fluid cell wall. For simplicity, hereafter we refer to this force as either attraction or repulsion based on its direction towards the fluid cell wall.

The motion of a particle in a fluid has been studied extensively in the past. Stokes [9], Boussinesq [10], and Basset [11] derived expressions for the forces affecting the motion of a particle submerged in a fluid subjected to harmonic and arbitrary motions. An equation of motion for a small rigid sphere in a nonuniform flow was previously developed by Maxey and Riley [12]. Chelomey [13] reported that for solid particles immersed in a liquid-filled container subjected to vibrations, particles heavier than the surrounding fluid could emerge at the top while particles lighter than the fluid could move downward. He considered nonuniform forces arising from the vibrations to be responsible for this paradoxical behavior. More recently, an analytical model was developed by Coimbra and Rangel [14] for the periodic motion of a small particle in a viscous fluid. Their model accounted for virtual mass, Stokes drag, and history forces. This model was later confirmed experimentally by Coimbra *et al.* [15] and L'Esperance *et al.* [16].

Hassan *et al.* [17,18] and Hassan and Kawaji [19,20] investigated the vibration-induced motions of a particle in a water-filled fluid cell. Under the vibration conditions examined, water could be considered inviscid. Hassan *et al.* [21] conducted analytical and experimental studies and reported the existence of an attraction force acting on a particle vibrating near a wall for an inviscid fluid cell. This vibration-induced attraction force was reported to push the plane of the oscillating particle towards the nearest cell wall. Hassan and Kawaji [22] also investigated both analytically and experimentally the vibration-induced oscillation of a particle in a viscous fluid. They found the amplitude of the particle oscillating in a viscous fluid to be dependent on the fluid viscosity and particle diameter. However, they did not examine the vibration-induced attraction or repulsion force in a viscous fluid cell.

Simic-Stefani *et al.* [8] numerically investigated the effect of small vibrations on a particle in a fluid cell under zero

*msaadatmand@ccny.cuny.edu

†Corresponding author: kawaji@ecf.utoronto.ca

gravity and reported that six parameters could affect the particle motion; the cell vibration frequency and amplitude, particle diameter and density, and fluid viscosity and density. However, they did not include the effects of the nearest cell wall on the particle oscillation in their study. In a somewhat related study, Klotsa *et al*. [23] studied the interaction of two spheres placed close together in an oscillating fluid cell filled with glycerol-water mixtures of three kinematic viscosities ranging from 2.0×10^{-6} to 9.4×10^{-6} $m^2\,s^{-1}$ and reported a rapid attraction of the spheres upon the start of the vibrations.

Lyubimov *et al*. [24] conducted analytical and numerical studies on a drop or bubble in a pulsating flow near each other or a rigid wall surface. They found that for parallel and normal vibration orientations the drop would be attracted to the wall. For two similar drops, repulsion was predicted to occur for vibrations directed along the line connecting the drop centers, and attraction for vibrations perpendicular to the line between the drops. Lyubimov *et al*. [24], however, did not report on the effects of viscosity and density of the fluid on the interactions of the drops or bubbles. In a more recent work, Lyubimova *et al*. [25] conducted a numerical study on the vibration-induced bubble motion in low viscosity fluids under zero gravity and reported the attraction of the bubble to the nearest wall or another bubble nearby for vibrations parallel to the wall or perpendicular to the line connecting the bubble centers.

Saadatmand *et al*. [26,27] studied the mechanisms that cause attraction of a particle to the nearest wall in an inviscid fluid cell under zero gravity, by conducting three-dimensional direct numerical simulations. They reported that the attraction force on the particle is related to Bernoulli's principle of reduced pressure in the gap between the particle and the fluid cell wall. In another numerical investigation, Liang *et al*. [28] confirmed this behavior for a bubble near the wall of a fluid cell.

Recently, Saadatmand and Kawaji [29] investigated experimentally the effect of viscosity on vibration-induced motion of a particle in a fluid cell. They observed a repulsion force on a particle oscillating near the cell wall, which caused the plane of the oscillating particle to move away from the cell wall. The repulsion force was found to increase with increases in the fluid viscosity and cell vibration amplitude and frequency.

The objective of the present work is to determine the physical mechanism responsible for the repulsion of a particle from a nearby wall of a fluid cell, while the cell is vibrating under zero gravity. To this end direct numerical simulations have been performed in three dimensions (3D) for a particle suspended in a fluid cell subjected to sinusoidal vibrations of known amplitude and frequency. The results of the numerical simulations show how the flow and pressure fields around the particle would give rise to the repulsion force.

II. NUMERICAL SIMULATION

The direct numerical simulation code used in this work is PARTFLOW3D, developed by Hu *et al*. [30] for 3D simulations. The code can simulate the motion of solid particles in a fluid cell. The description of the code given below is mainly taken from Hu *et al*. [30] where more detailed information can be found. The code is based on a finite-element technique and solves the equations of motion for both the fluid and particle which are combined into a single equation of motion. PARTFLOW3D can consider the motions of N rigid solid particles in an incompressible fluid. It also considers a fluid domain, $\Omega_0(t)$, at a given time t, and domain of particles $\Omega_i(t)$, where the index i $(=1, 2, \ldots, N)$ represents different solid particles.

PARTFLOW3D uses a mesh composed of unstructured tetrahedron elements. This type of mesh is suitable for the irregularity and movement of the domain. Since the nodes on the particle surface move with the particle, the code has to solve a moving boundary problem. To do this, the mesh is regenerated at each time step. The code is based on an arbitrary Lagrangian-Eulerian technique, which uses the standard Galerkin finite-element method. At each time step, the positions of the particle and the mesh are updated explicitly, while the velocities of the particle and fluid are determined implicitly.

A. Governing equations

The governing equations for the fluid motion solved in PARTFLOW3D are the conservation of mass and momentum. The governing equations for the rigid particles are Newton's second law for the translational motion, and the Euler equations for the rotation. In this work, the motion of a particle in a sinusoidally vibrated fluid cell was predicted. In a fixed frame of reference, the cell acceleration can be specified through the body force $\mathbf{f}$ defined as

$$\mathbf{f} = \mathbf{g_s} - A_c\omega^2 \sin(\omega t), \tag{1}$$

where $\mathbf{g}_s$ represents a steady residual acceleration, A_c is the cell vibration amplitude (half of peak to peak), and ω is the angular frequency $(=2\pi f)$. The residual acceleration was assumed to be zero in this work. The nonslip boundary condition on the particle surface was given by

$$\mathbf{u} = \mathbf{V}_i + \boldsymbol{\omega}_i \times (\mathbf{x} - \mathbf{X}_i), \tag{2}$$

where $\mathbf{u}$ is the velocity of the fluid, $\mathbf{V}_i$ is the velocity of the particle, $\boldsymbol{\omega}_i$ is the angular velocity of the particle, $\mathbf{X}_i$ is the position of the sphere centroid, and $\mathbf{x}$ is the position of a given point on the particle surface. For the cell walls which form the boundaries of the computational domain, the nonslip boundary condition was

$$\mathbf{u} = \mathbf{0}. \tag{3}$$

To use the finite-element method, Hu *et al*. [30] derived a weak formulation that incorporated both the fluid and particle equations of motion. The weak formulation was derived by multiplying the momentum equation by a test function for the fluid velocity, $\tilde{\mathbf{u}}$, and integrating over the fluid domain at time t. This test function would be replaced by Eq. (2) for the particles. Finally, the combined fluid-particle momentum equation would have the following form:

$$\begin{aligned}&\int_{\Omega_0} \rho_f \left(\frac{D\mathbf{u}}{Dt} - \mathbf{f}\right) \cdot \tilde{\mathbf{u}} d\Omega \\ &\quad + \int_{\Omega_0} \sigma : \mathbf{D}[\tilde{\mathbf{u}}] d\Omega + \sum_{1 \leqslant i \leqslant N} \tilde{\mathbf{V}}_i \cdot \left(m_i \frac{d\mathbf{V}_i}{dt} - \mathbf{G}_i\right) \\ &\quad + \sum_{1 \leqslant i \leqslant N} \tilde{\omega}_i \cdot \frac{d(\mathbf{I}_i \omega_i)}{dt} = 0,\end{aligned} \tag{4}$$

where ρ_f is the density of the fluid, Ω is the computational domain, σ is the stress tensor, m_i is the mass, $\mathbf{V}_i$ is the translational velocity of the ith particle, $\mathbf{G}_i$ is the external body force, and $\mathbf{I}_i$ is the moment of inertia matrix.

For the fluid-particle system, as is clear from Eq. (4), the forces and moments acting on the particle do not explicitly appear in the formulation. By considering the fluid and particles as one system, forces related to the fluid turn to internal forces in the formulation. Combining the momentum equations of the fluid and particle reduces the computational time, and is an advantage for numerical computation of the fluid and particle behaviors.

B. Code validation against an approximate analytical solution

To confirm the accuracy of the numerical code, simulation results were first compared with an analytical solution to Tchen's [31] equation of motion for the stationary regime. Tchen [31] extended the BBO (Basset [11], Boussinesq [10], and Oseen [32]) equation to the case of a fluid moving with a variable velocity. Tchen [31] studied the case of a uniform time-dependent free stream and modified the BBO equation as follows:

$$\frac{\pi}{6}D_0^3\rho_p\frac{dV}{dt} = 3\pi\mu D_0(u-V) + \frac{\pi}{6}D_0^3\rho_f\frac{du}{dt} + \frac{1}{2}\frac{\pi}{6}D_0^3\rho_f\left(\frac{du}{dt}-\frac{dV}{dt}\right) + \frac{3}{2}D_0^2\sqrt{\pi\rho_f\mu} \times \int_{t_0}^{t}\frac{du/d\tau - dV/d\tau}{\sqrt{t-\tau}}d\tau + F_e. \quad (5)$$

In Eq. (5), t_0 is the starting time, ρ_f and ρ_p are fluid and particle densities, respectively, μ is the dynamic viscosity of the fluid, u is the fluid velocity in the neighborhood of the particle, and V is the instantaneous velocity of the particle.

Tchen's [31] equation is valid only for infinitesimal particle Reynolds numbers ($\mathrm{Re} = \rho_f A_p \omega D_o/\mu$) in unsteady uniform background flows. In spite of this limitation, the solution to Eq. (5) is used here as an approximate solution for the particle movement, to be compared with the results of the PARTFLOW3D simulations. In the solution previously presented by Tchen [31], Hinze [33], Hjelmfelt and Mockros [34], and Coimbra and Rangel [14], the velocities of the fluid and the particle were expressed as sinusoidal functions, and the particle-to-fluid amplitude ratio, η, in the cell frame of reference was given.

To validate the results of the present numerical simulations, the particle-to-fluid amplitude ratio was calculated using the solution for Tchen's equation of motion given by Coimbra and Rangel [14] and compared with the results obtained from PARTFLOW3D simulations. Figure 1 shows a comparison for the case of a 4.0-mm-diameter stainless steel particle suspended in a viscous fluid cell vibrated at a frequency of 10 Hz and amplitude of 2.0 mm under zero gravity environment. To obtain different Reynolds numbers, the dynamic viscosity of the fluid was changed from 0.126 to 10 Pa s, while the density of the fluid was kept constant at 1000 kg/m^3. As this figure shows, at low Reynolds numbers, the particle-to-fluid amplitude ratio, η, obtained from the simulations is in close agreement with the analytical results. The difference between η calculated from the analytical solution and the simulations is 1.1% for the lowest Reynolds number but increased to 9.0% for $\mathrm{Re} = 2.15$. As previously stated, since Tchen's equation is valid only for very low Reynolds numbers, the present results suggest that the simulations and analytical solution are in close agreement for low Reynolds numbers. Therefore, the numerical model used in this work is considered to be valid with respect to the particle-to-cell amplitude ratio [35].

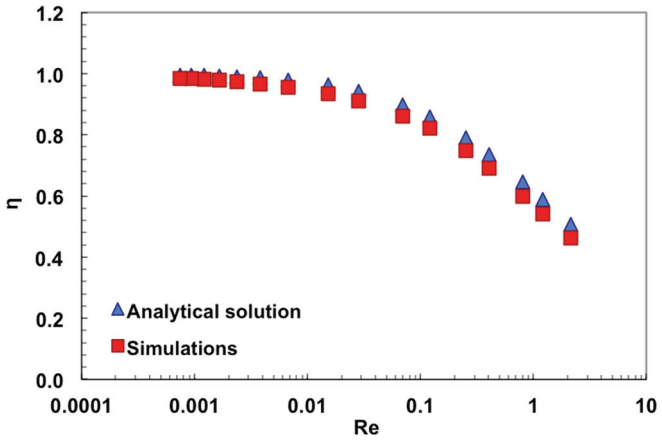

FIG. 1. (Color online) Comparison of particle amplitude η obtained from simulations and analytical solution for a 4.0-mm-diameter stainless steel particle. Re was calculated for a fluid of density 1000 kg/m^3 and viscosity of 0.126–10 Pa s. The fluid cell was subjected to 10-Hz sinusoidal vibrations with a 2.0-mm cell amplitude.

III. RESULTS AND DISCUSSION

A. Physical mechanism of repulsion force

Saadatmand *et al.* [27] conducted numerical simulations to investigate the mechanisms of attraction force on a particle in a nearly inviscid fluid. They reported that the particle would be attracted towards the cell wall based on Bernoulli's principle of reduced pressure in high-velocity zones of the flow, mainly in the gap between the particle and the nearest wall. In the present work, numerical simulations have been conducted to understand the mechanism of the repulsion force experienced by a particle oscillating near a cell wall in highly viscous fluids.

In the simulations the particle was initially placed near one of the vertical cell walls of a fluid cell as shown in Fig. 2. As the cell was vibrated in the z direction with a specified amplitude and frequency, the particle was also induced to oscillate in the same direction, parallel to the nearest wall. First, the particle was fixed in the y direction (perpendicular to the nearest wall) in the simulations to better study the repulsion force acting on the particle. If the particle is allowed to move away from the wall, the magnitude of the repulsion force would change with the distance between the particle and the wall.

In the simulations, a 12.7-mm-diameter stainless steel particle was placed very close to one of the cell walls (Fig. 2) with its centroid at $x = 76.0$ mm, $y = 42.73$ mm, and $z = 25.0$ mm, so that the distance between the edge of the particle and the nearest cell wall, δ, was 0.92 mm. The fluid cell was subjected to sinusoidal vibrations of 1.0-mm amplitude (half of peak to peak) and two different frequencies of 7.0

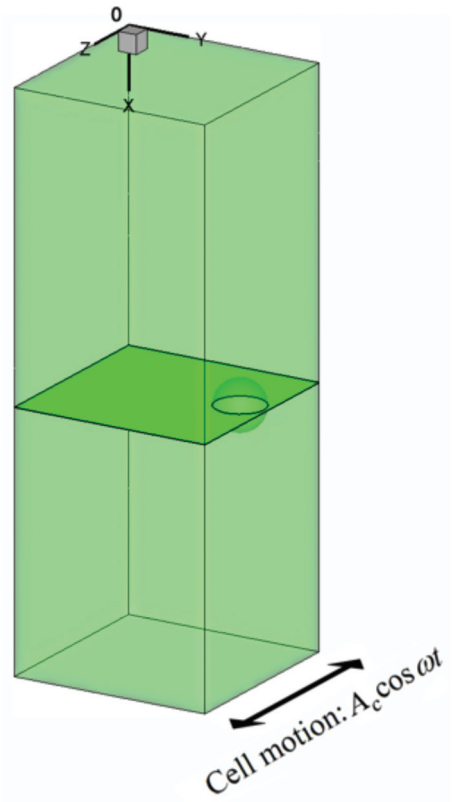

FIG. 2. (Color online) Schematic of the fluid cell and particle showing the horizontal plane for flow visualization.

and 15 Hz. All the numerical results were obtained with a sufficiently small mesh such that the results would not vary by more than 1% with further mesh refinement.

All the simulations were conducted in 3D, and the predicted velocity and pressure fields in the horizontal z-y plane that cuts through the centroid of the particle shown in Fig. 2 are discussed below to reveal the flow pattern around the particle. As shown in Fig. 3, there are four different zones of interest close to the particle: the front and back zones which lie in front and back of the moving particle, respectively, the wall zone between the particle and the nearest wall, and the fluid zone on the opposite side.

In one vibration cycle, the particle moves from $z = +A_p$ to $-A_p$ and then back to $z = +A_p$, where A_p is half of the peak-to-peak amplitude of the oscillating particle. To discuss the results of simulations of the particle movement in the fluid cell, let us consider five different positions of the particle in one half of a vibration cycle (Fig. 3):

Position 1. The particle is moving in $-z$ direction with its maximum velocity.

Position 2. The particle is halfway towards its end position ($z = -A_p/2$).

Position 3. The particle reaches the end position ($z = -A_p$) and its velocity is zero.

Position 4. The particle is moving in $+z$ direction and is halfway to its equilibrium position ($z = 25$ mm).

Position 5. The particle is moving in $+z$ direction and reaches its maximum velocity at $z = 25$ mm.

The flow patterns predicted are shown and discussed below for the particle Positions 1–5 for a cell vibration amplitude of 1.0 mm and frequencies of 7.0 and 15 Hz. The units of velocity and pressure are cm/s and g/cm s^2, respectively.

B. Pressure variations and repulsion force in a 1000-cS fluid

Figures 4 and 5 show the fluid motion and pressure distributions around the moving particle as found from the simulations at five particle positions for two frequencies of 15 and 7.0 Hz, respectively. At Position 1, the particle is moving with the highest velocity in $-z$ direction [downward in Figs. 4(a) and 5(a)], and the fluid velocity in the wall zone is lower than in the fluid zone. The particle is pushing the fluid in front to move away from the wall, which causes the formation of a vortex in the fluid zone. Also, near the wall, the pressure rises in front of the particle but decreases in the rear. Since a pressure difference between the wall and fluid zones would give rise to an attraction or repulsion force in the y

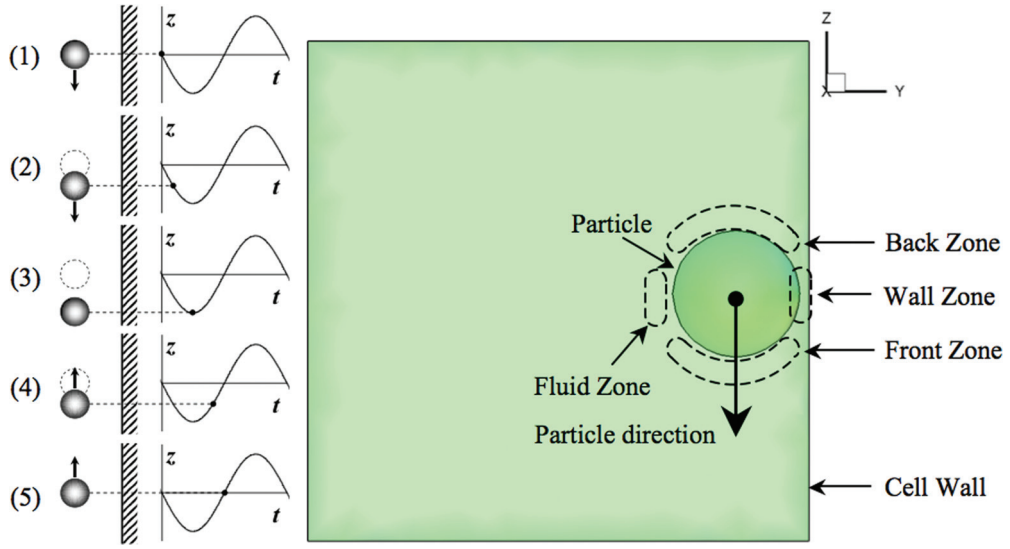

FIG. 3. (Color online) A top view of different zones around the particle in a horizontal plane passing through the centroid of the particle. Particle Positions 1–5 are defined during a half of the oscillation cycle. The right part of the figure corresponds to Position 1 ($z = 25$ mm).

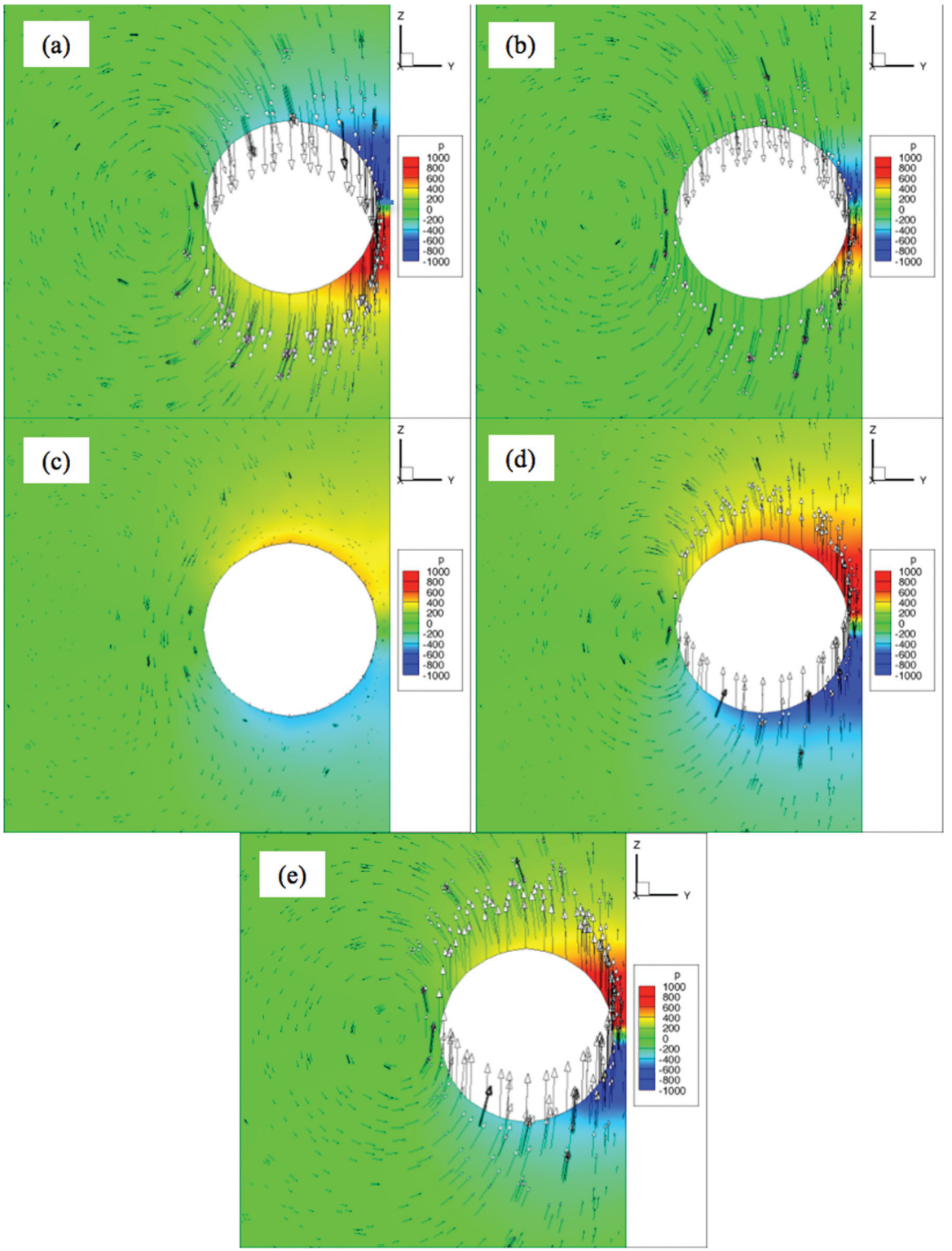

FIG. 4. (Color online) Velocity and pressure distributions around a 12.7-mm-diameter stainless steel particle for a cell amplitude of 1.0 mm and frequency of 15.0 Hz (viscosity = 1000 cS, $\delta = 0.92$ mm); (a) Position 1, (b) Position 2, (c) Position 3, (d) Position 4, (e) Position 5 (the units of velocity and pressure are cm/s and g/cm s^2, respectively).

direction, the front half of the particle experiences a repulsion force which would push the particle away from the wall. On the other hand, the rear half of the particle experiences an attraction force, but a film of high-viscosity liquid between the particle and the wall would hinder the movement of the particle towards the wall. Thus, the pressure variations generated by the particle motion at Position 1 would result in repulsion of the particle away from the nearest wall.

At Position 2 [Figs. 4(b) and 5(b)] halfway to the end position, the flow pattern around the particle remains similar

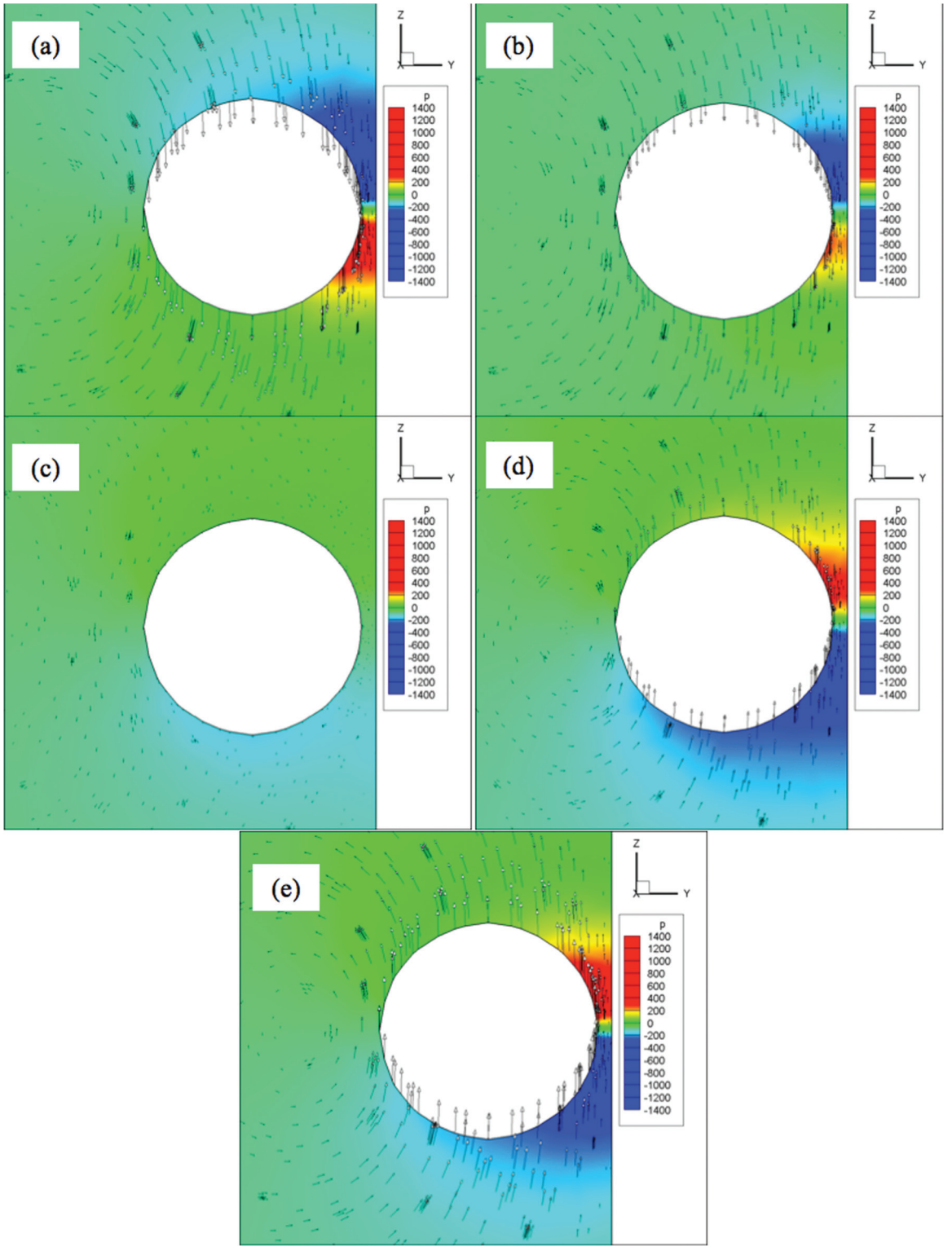

FIG. 5. (Color online) Velocity and pressure distributions around a 12.7-mm-diameter stainless steel particle for a cell amplitude of 1.0 mm and frequency of 7.0 Hz (viscosity = 1000 cS, $\delta = 0.92$ mm); (a) Position 1, (b) Position 2, (c) Position 3, (d) Position 4, (e) Position 5 (the units of velocity and pressure are cm/s and g/cm s^2, respectively).

to that shown in Figs. 4(a) and 5(a). However, the velocity and pressure variations around the particle are reduced compared to those at Position 1. At Position 3 [Figs. 4(c) and 5(c)], the particle reaches the end of its oscillation trajectory and comes to rest momentarily. The fluid velocity is everywhere reduced and the fluid velocity in the wall zone is even lower than in the other zones. As a result, the pressure variation around the particle is reduced and the pressure difference in the y direction reaches its smallest value.

At Position 4 [Figs. 4(d) and 5(d)], the particle and fluid motions are similar to those at Position 2, except that the direction of the particle motion is reversed. Similar to Positions 1 and 2, some parts of the wall zone and the front zone show higher pressures. The high-pressure zone is mostly located between the front half of the particle and the wall, which again results in a repulsion force. Finally at Position 5 [Figs. 4(e) and 5(e)], the velocity and pressure variations around the particle are similar to those at Position 1 but the particle is moving in the opposite direction.

Note that due to the high viscosity of the fluid in this study, the Reynolds number for the flow in the gap between the particle and the wall ($\mathrm{Re} = \rho_f u l/\mu$) is quite low. The Reynolds number calculated at Position 5, based on the distance between the particle and the wall, and the average velocity of the fluid in the gap region was 0.012 and 0.0085 for frequencies of 15 and 7 Hz, respectively.

C. Relation between repulsion force and particle velocity

Figures 6 and 7 show the variation of the repulsion force exerted on the 12.7-mm steel particle in a 1000-centistokes (cS) fluid for a cell amplitude of 1.0 mm and frequencies of 7.0 and 15 Hz. Moreover, Fig. 8 shows the variations of the repulsion force and velocity for a 4.0-mm-diameter steel particle. This is the case corresponding to the particle shown in Fig. 1. For this case, the cell was subjected to sinusoidal vibrations of 10-Hz frequency and 2.0-mm cell amplitude, and the edge of the particle was located at $\delta = 0.1$ mm from the cell wall. The fluid viscosity was chosen to be 420 cS so that the Reynolds number would be equal to the case of the 12.7-mm-diameter particle at 15 Hz frequency. As these figures show, the velocity peaks occur when the particle crosses the vertical plane at $z = 25$ mm. A negative force in the y direction represents a repulsion force away from the nearest cell wall. The maximum magnitude of the repulsion force is obtained shortly after the particle velocity reaches its maximum at Positions 1 and 5. The minimum repulsion force occurs shortly after the particle reaches its end of the trajectory and comes to rest momentarily.

A time lag exists between the particle velocity and repulsion force because the fluid motion around the particle also lags behind the particle motion. In all cases shown, it is apparent that the vibration of a viscous fluid cell induces a repulsion force that always pushes the particle away from the nearest wall.

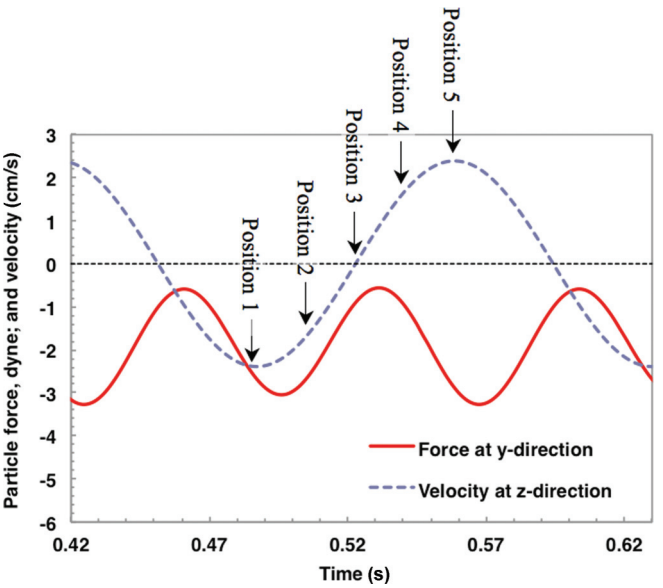

FIG. 7. (Color online) Velocity and repulsion force in y direction for a 12.7-mm-diameter stainless steel particle and cell vibration amplitude of 1.0 mm and frequency of 7 Hz (viscosity = 1000 cS, $\delta = 0.92$ mm).

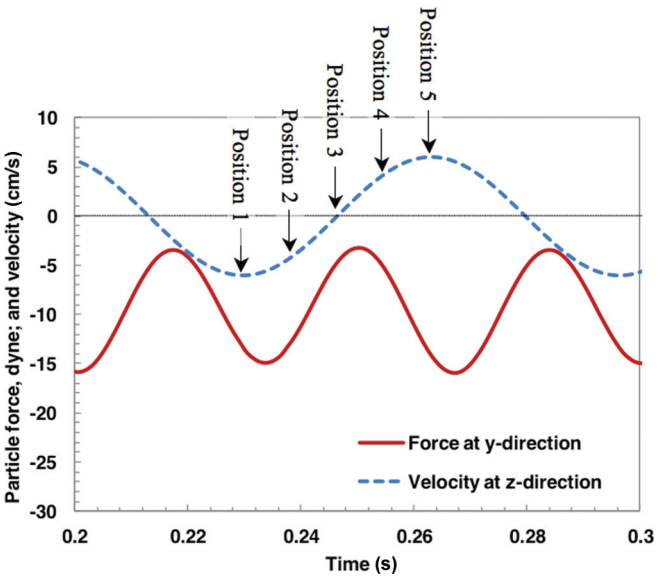

FIG. 6. (Color online) Velocity and repulsion force in y direction for a 12.7-mm-diameter stainless steel particle and cell vibration amplitude of 1.0 mm and frequency of 15 Hz (viscosity = 1000 cS, $\delta = 0.92$ mm).

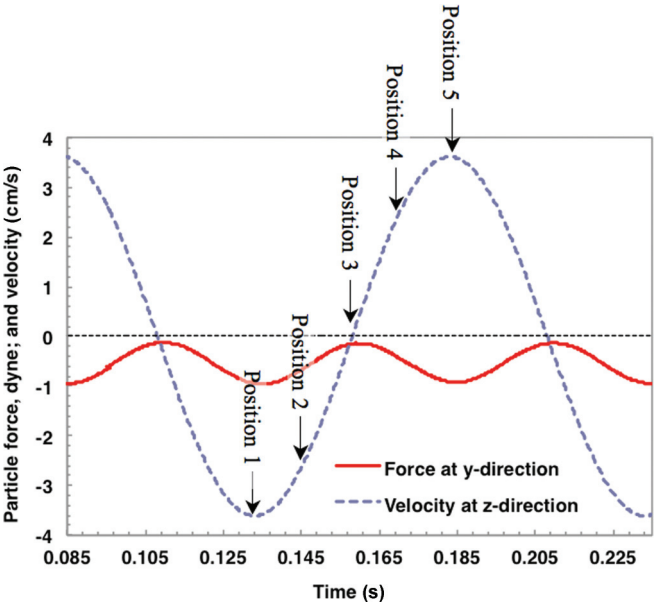

FIG. 8. (Color online) Velocity and repulsion force in y direction for a 4.0-mm-diameter stainless steel particle and cell vibration amplitude of 2.0 mm and frequency of 10.0 Hz (viscosity = 1000 cS, $\delta = 0.1$ mm).

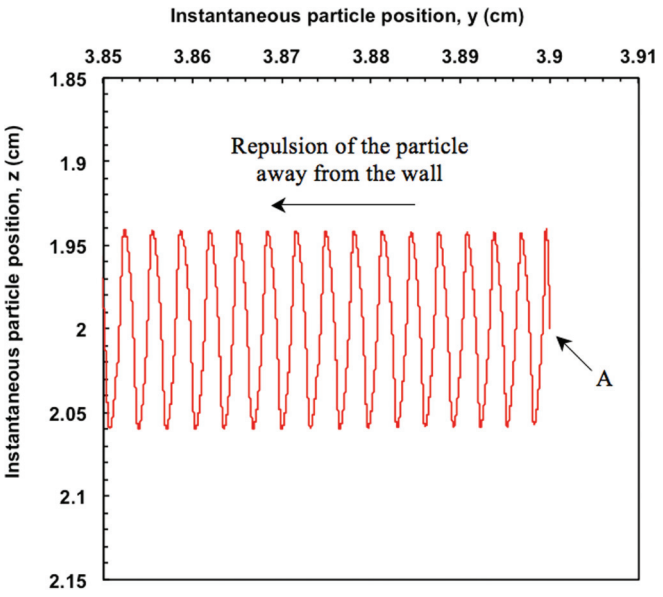

FIG. 9. (Color online) Trajectory of the centroid of a free-floating particle in y-z plane where the fluid cell wall is located on the right-hand side. The particle starts from the point A when the fluid cell is at rest and drifts away from the nearest wall after the start of the vibrations. (1.0-mm-diameter stainless steel particle, ρ_p =7900.0 kg/m^3, $\rho_f = 1000.0$ kg/m^3, $f = 10$ Hz, $\nu = 44.3$ cS, $\delta = 0.5$ mm, cell amplitude = 2.0 mm).

The velocity and pressure fields presented in Figs. 4 and 5 show that the vibration of the fluid cell filled with a viscous fluid gives rise to a repulsion force on the particle as shown in Figs. 6 and 7 which would push the particle away from the nearest wall. To study the response of the particle to the repulsion force, a simulation was conducted for a 1.0-mm-diameter stainless steel particle in a fluid cell without constraining the particle motion in the $-y$ direction. The fluid viscosity was 44.3 cS and the edge of the particle was initially located at a distance of $\delta = 0.5$ mm from the nearest wall. As shown in Fig. 9, the centroid of the particle follows a zigzag trajectory starting from the initial position A and moving away from the wall as it oscillates in parallel with the nearest wall.

IV. CONCLUSIONS

To investigate the mechanism of a vibration-induced repulsion force on the particle from the nearest wall in a fluid cell, 3D direct numerical simulations were conducted for spherical stainless steel particles of 12.7, 4.0, and 1.0 mm diameter in a sinusoidally vibrated fluid cell filled with a viscous fluid of 1000 and 44.3 cS viscosity and 1000 kg/m^3 density under zero gravity. The simulations performed for different cell vibration amplitudes and frequencies predicted a repulsion force pushing the particle away from the nearest cell wall. The simulations also revealed that the pressure between the front half of the particle and the nearest wall is higher than in other regions inside the fluid cell. Moreover, the lowest fluid velocity was predicted to occur in the gap between the particle and the nearest wall due to the high viscosity of the fluid. Since the highest pressure in the fluid cell is reached in the area between the front half of the particle and the wall, the particle experiences a strong repulsion force, which directs the particle to move away from the wall. Thus, the numerical simulation results for a highly viscous fluid suggest that the repulsion force on the particle is due to a pressure rise in the region between the front half of the particle and the nearest cell wall. These results are opposite to the high velocity and reduced pressure in the gap between the particle and the nearest wall predicted for an inviscid fluid, which would give rise to an attraction force [27].

ACKNOWLEDGMENTS

The authors would like to thank the Canadian Space Agency for an SSEP grant to financially support this work. We would also like to thank Professor Howard H. Hu at University of Pennsylvania for providing the PARTFLOW3D code and helping the authors in the use of this code.

[1] N. E. Chayen, E. H. Snell, J. R. Helliwell, and P. F. Zagalsky, J. Cryst. Growth **171**, 219 (1997).
[2] B. Lorber, J. D. Ng, P. Lautenschlager, and R. Giegé, J. Cryst. Growth **208**, 665 (2000).
[3] S. Ostrach, Annu. Rev. Fluid Mech. **14**, 313 (1982).
[4] W. Knabe and D. Eilers, Acta Astronaut. **9**, 187 (1982).
[5] K. Jules, K. McPherson, K. Hrovat, E. Kelly, and T. Reckart, Acta Astronaut. **55**, 335 (2004).
[6] S. Shafie, N. Amin, and I. Pop, Mech. Res. Commun. **34**, 115 (2007).
[7] M. Kawaji, O. Gamache, D. H. Hwang, N. Ichikawa, J. P. Viola, and J. Sygusch, J. Cryst. Growth **258**, 420 (2003).
[8] S. Simic-Stefani, M. Kawaji, and H. H. Hu, J. Cryst. Growth **294**, 373 (2006).
[9] G. G. Stokes, Cambridge Philos. Trans. **9**, 8 (1851).
[10] J. Boussinesq, C. R. Acad. Sci. Paris **100**, 935 (1885).
[11] A. B. Basset, *A Treatise on Hydrodynamics* (Deighton, Bell and Co Press, Cambridge, UK, 1888), Chap. 21, pp. 260–284.
[12] M. R. Maxey and J. J. Riley, Phys. Fluids **26**, 883 (1983).
[13] V. N. Chelomey, Acta Astronautica **11**, 269 (1984).
[14] C. F. M. Coimbra and R. H. Rangel, AIAA J. **39**, 1673 (2001).
[15] C. F. M. Coimbra, D. L'Esperance, and R. A. Lambert, J. Fluid Mech. **504**, 353 (2004).
[16] D. L'Esperance, C. F. M. Coimbra, and J. D. Trolinger, Exp. Fluids **38**, 112 (2005).
[17] S. Hassan, T. P. Lyubimova, D. V. Lyubimov, and M. Kawaji, Int. J. Multiphase Flow **32**, 1037 (2006).
[18] S. Hassan, T. P. Lyubimova, D. V. Lyubimov, and M. Kawaji, J. Appl. Mech. **73**, 72 (2006).
[19] S. Hassan and M. Kawaji, AIAA J. **45**, 2090 (2007).
[20] S. Hassan and M. Kawaji, Microgravity Sci. Technol. **19**, 109 (2007).
[21] S. Hassan, M. Kawaji, T. P. Lyubimova, and D. V. Lyubimov, J. Appl. Mech. **73**, 610 (2006).
[22] S. Hassan and M. Kawaji, J. Appl. Mech. **75**, 031012 (2008).

[23] D. Klotsa, M. R. Swift, R. M. Bowley, and P. J. King, Phys. Rev. E **76** 056314 (2007).

[24] D. Lyubimov, T. P. Lyubimova, and S. V. Shklyaev, *Proceedings of the First International Symposium on Microgravity Research and Applications in Physical Sciences and Biotechnology, 10–15 September 2000, Sorrento, Italy* (ESA Publications Division, European Space Agency, Noordwijk, The Netherlands, 2001), pp. 879–886.

[25] T. Lyubimova, A. Cherepanova, and L. Filippov, J. Phys.: Conf. Ser. **416**, 012030 (2013).

[26] M. Saadatmand, M. Kawaji, and H. H. Hu, *Proceedings of the 7th International Conference on Multiphase Flow, ICMF 2010, 30 May–9 June 2010, Tampa, FL* (University of Florida, Gainesville, Florida, 2010).

[27] M. Saadatmand, M. Kawaji, and H. H. Hu, Microgravity Sci. Technol. **24**, 53 (2012).

[28] R. Liang, D. Liang, F. Yan, Z. Liao, and G. Duan, Microgravity Sci. Technol. **23**, 79 (2011).

[29] M. Saadatmand and M. Kawaji, Microgravity Sci. Technol. **22**, 433 (2010).

[30] H. H. Hu, N. A. Patankar, and M. Y. Zhu, J. Comput. Phys. **169**, 427 (2001).

[31] C. M. Tchen, Ph.D. thesis, Technical University of Delft, 1947.

[32] C. Oseen, Ark. Mat., Astron. Fys. **6**, 29 (1910).

[33] O. Hinze, *Turbulence* (McGraw-Hill, New York, 1975).

[34] A. T. Hjelmfelt, Jr. and L. F. Mockros, Appl. Sci. Res. **16**, 149 (1966).

[35] M. Saadatmand, Ph.D. thesis, University of Toronto, 2012.